Sun, Z., Jian, Z., Stock, J.M., Larsen, H.C., Klaus, A., Alvarez Zarikian, C.A., and the Expedition 367/368 Scientists
Proceedings of the International Ocean Discovery Program Volume 367/368
publications.iodp.org

Data report: marine tephra compositions in the deep drilling cores of the South China Sea, IODP Expeditions 349 and 367/368[1]

J.C. Schindlbeck-Belo,[2] Kelsie Dadd,[3] Kuo-Lung Wang,[4,5] and Hao-Yang Lee[4]

[1] Schindlbeck-Belo, J.C., Dadd, K., Wang, K.-L., and Lee, H.-Y., 2022. Data report: marine tephra compositions in the deep drilling cores of the South China Sea, IODP Expeditions 349 and 367/368. In Sun, Z., Jian, Z., Stock, J.M., Larsen, H.C., Klaus, A., Alvarez Zarikian, C.A., and the Expedition 367/368 Scientists, South China Sea Rifted Margin. Proceedings of the International Ocean Discovery Program, 367/368: College Station, TX (International Ocean Discovery Program). https://doi.org/10.14379/iodp.proc.367368.204.2022
[2] GEOMAR Helmholtz Centre for Ocean Research Kiel, Germany. Correspondence author: **jbelo@geomar.de**
[3] School of Geosciences, University of Sydney, Sydney, Australia.
[4] Institute of Earth Sciences, Academia Sinica, Taipei, Taiwan.
[5] Department of Geosciences, National Taiwan University, Taipei, Taiwan.

Contents

Keywords
International Ocean Discovery Program, IODP, *JOIDES Resolution*, Expedition 367/368, South China Sea Rifted Margin, tephra, glass

Supplementary material

References (RIS)

MS 367368-204
Received 7 June 2022
Accepted 29 August 2022
Published 14 October 2022

Abstract

We present geochemical major and trace element glass data for tephra samples from International Ocean Discovery Program (IODP) Expeditions 349 and 367/368 from four drilling sites in the South China Sea. Overall, we obtained data for 55 samples and identified 46 as tephra layers, with dominant volcanic glass shards in the component inventory (in the 63–125 μ fraction). In total, we performed 720 single glass shard analyses using an electron microprobe for major element compositions, as well as 130 single glass shard analyses using laser ablation–inductively coupled plasma–mass spectrometry (LA-ICP-MS) for trace element compositions. The compositions of the samples range from basaltic, (trachy-) andesitic to trachytic, and rhyolitic and fall mainly into the calc-alkaline and K-rich calc-alkaline magmatic series. One sample falls into the shoshonitic series. Tephras from Expedition 349 Site U1431 span the whole compositional range, whereas tephras from the other sites are limited to rhyolitic composition. Tephra ages, calculated applying sedimentation rates, range to ~2 Ma at Site U1431, ~0.8 Ma at Expedition 367 Site U1499, ~0.6 Ma at Expedition 368 Site U1501, and ~0.9 Ma at Expedition 368 Site U1505.

1. Introduction

The South China Sea (SCS) was the target area of Ocean Drilling Program (ODP) Leg 184 in 1999, International Ocean Discovery Program (IODP) Expedition 349 in 2014, and IODP Expedition 367/368 in 2017. The aim of these expeditions was to study the tectonic and sedimentary history of the different subbasins in the SCS (Figure **F1**). In this data report, we present geochemical data for tephra layers from the three IODP expeditions. We report on single glass shard analyses of major and trace elements of discrete tephra layers from these expeditions. Data on the compositions of the discrete layers can be used to evaluate their primary, eruption-related versus secondary, reworked origin and to correlate between sites and with onshore tephra samples. Marine tephra layers correlated to specific eruptions on land are valuable independent time markers.

1.1. Geological overview

The SCS is a large basin in eastern Asia located in a tectonically complex area at the junction of the Eurasian, Australian, Indian, and Pacific plates. It is a relatively young (mid- to late Cenozoic) oceanic basin that formed along the eastern boundary of the Eurasian plate, and its initial formation is highly debated (e.g., Li et al., 2013; Sun, 2016; Franke et al., 2014; Xu et al., 2012; Barckhausen et al., 2014). The continental crust that was rifted to form the SCS was accreted to the Asian margin

during the Mesozoic (Zhou and Li, 2000; Zhou et al., 2008; Li et al., 2012; Li and Song, 2012) and underwent extensive rifting during the Eocene and Oligocene. Seafloor spreading in the northern SCS started during the Oligocene (~29.5–31 Ma; Briais et al., 1993; Li et al., 2013, 2014; Franke et al., 2014) and expanded to the southwest SCS from ~23 Ma.

Subduction of the eastern part of the SCS started in the early Miocene along the Manila Trench (Li et al., 2013; Franke et al., 2014), which is also the timing for the commencement of volcanism along the west side of Luzon (Pubellier et al., 2000). After about 16–15 Ma, seafloor spreading in the SCS ceased (Li et al., 2015a). The cessation is thought to be related to the initiation of the Palawan/Mindoro–Central Philippines collision event (e.g., Yumul et al., 2003) as well as the final closure of the Borneo wedge that blocked the subduction zones in the southeastern and southern part of the SCS. Today, subduction is limited to the Manila Trench, which extends over 900 km from Mindoro to Taiwan (Figure **F1**).

The marine sediment record of the SCS basin records terrestrial input from diverse source regions (e.g., South China, Indochina, Borneo, Sumatra, Taiwan, Philippines) (Figure **F1**), including volcanic input from active volcanic regions, especially from the Philippine and Sumatra volcanic arcs (e.g., Ku et al., 2008, 2009).

1.2. Expedition overview

Expedition 349 drilled five sites, three in the central part of the SCS (Sites U1431, U1433, and U1434) and two in the northern part (Sites U1432 and U1435) (Figure **F1**) (Li et al., 2015b). At all sites, the major expedition goal was to reach the basement to better understand the processes of seafloor spreading, ocean crust accretion, and mantle evolution. A secondary objective was to study the overlying sediments because these provide important information about the sedimentary and paleoceanographic responses to basin opening and eventual subduction along the Manila Trench. At Site U1431, ~900 m of sediment was drilled overlying basaltic basement. The Pleistocene–Pliocene sediments at this site are dominated by clay and claystone, whereas the Miocene sediments are dominated by sandstone and breccia (Li et al., 2015b). Ash layers occur throughout the Pleistocene (Figure **F2**). At Site U1432, the basement was not reached and coring ended at 110 meters below seafloor (mbsf) (Li et al., 2015b). The Pleistocene sediments are dominated by clay interspersed with ash layers. The basaltic basement was reached at ~800 mbsf at Site

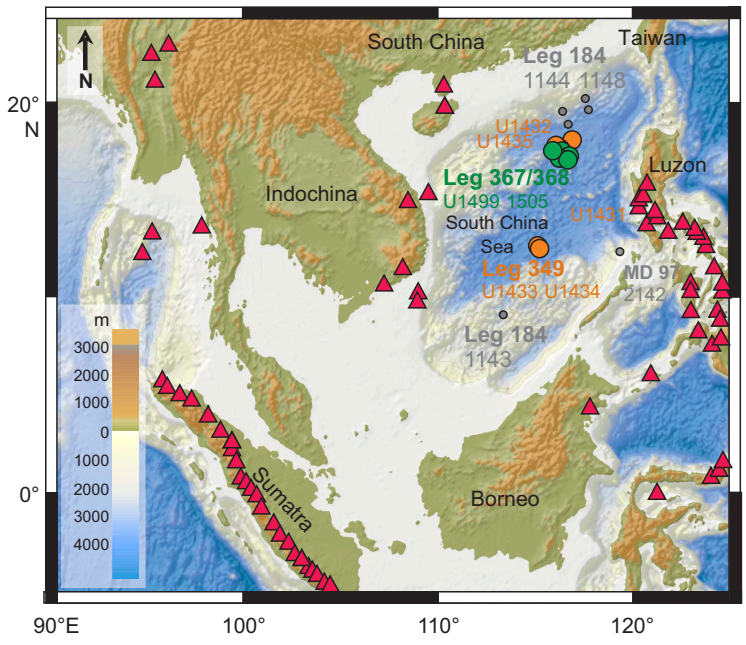

Figure F1. Overview map of the South China Sea and adjacent arcs. Colored dots mark the locations of ODP and IODP drill sites; red triangles indicate active volcanoes at adjacent arcs. Map created using GeoMapApp (**http://www.geomapapp.org**; GMRT-Global Multi-Resolution Topography; Ryan et al., 2009).

U1433. The overlying Pleistocene sediments are dominated by clay with few ash layers. From late Miocene to early Pleistocene, the clay is interbedded with carbonates (Li et al., 2015b). At Sites U1434 and U1435, recovery of young sediments was poor. However, only tephra samples from Hole U1431D have been investigated so far, and they are included in this data report.

Expedition 367/368 (**Larsen et al.**, 2018) drilled a transect across the SCS margin to understand the timing and process of rifting, eventual rupturing of the continental crust, and onset of the formation of igneous oceanic crust at a highly extended rifted margin. The drill sites cover a ~150 km wide continent–ocean transition zone (Sun et al., 2016) and targeted the four main tectonic features, the outer margin high and its small rift basins, and the three ridges within the distal margin (Ridges A, B, and C) (**Larsen et al.**, 2018).

Expedition 367/368 drilled at six sites (U1499–U1505) that are all located in the northern part of the SCS in vicinity to Sites U1432 and U1435. Site U1499 is located on Ridge A within the SCS continent–ocean transition about 60 km seaward and southeast of the outer margin high. A casing was installed down to 651 mbsf, followed by rotary coring to 1081.8 mbsf. A continuous sequence from Pleistocene nannofossil-rich clay and calcareous ooze to pre-Miocene sandstone and breccia was recovered (**Larsen et al.**, 2018). Site U1500 is located on Ridge B. The upper 378.2 m of sediment was drilled without coring, as was the interval from 494.6 to 641.2 mbsf. After installation of a casing, coring from 846.0 to 1379.1 mbsf recovered a sequence of Miocene clay- to sandstone overlying the basaltic basement. At Site U1501, located on the outer margin high, coring ~45 m into the acoustic basement sampled highly lithified sandstone to conglomerate of presumably Mesozoic age. This sequence is overlain by siliciclastic Eocene pre- to synrift sediments of Oligocene age and topped by primarily carbonaceous postrift sediments of early Miocene to Pleistocene age (**Larsen et al.**, 2018).

At Site U1502, a casing was installed to 723.7 mbsf, and the upper 380 m (Pliocene–Pleistocene) was not cored. The recovered 180 m of hydrothermally altered brecciated basalts are overlain by deep-marine sediments of Oligocene to late Miocene age (**Larsen et al.**, 2018). A 991.5 m casing was installed at Site U1503 in preparation for the planned deep drilling to ~1800 m, but no coring was performed because of mechanical problems (**Larsen et al.**, 2018). The basement recovered at Site U1504 is a metamorphic schist to gneiss (greenschist facies) that is overlain by Eocene carbonate rocks and early Miocene to Pleistocene sediments (**Larsen et al.**, 2018). Coring at Site U1505 recovered 480.15 m of Pleistocene to late Oligocene mainly carbonaceous ooze and early Oligocene to late Eocene siliciclastic sediments (**Larsen et al.**, 2018; Jian et al., 2018). Few discrete ash layers but numerous ash-rich horizons were described in the sediments cored at Sites U1501,

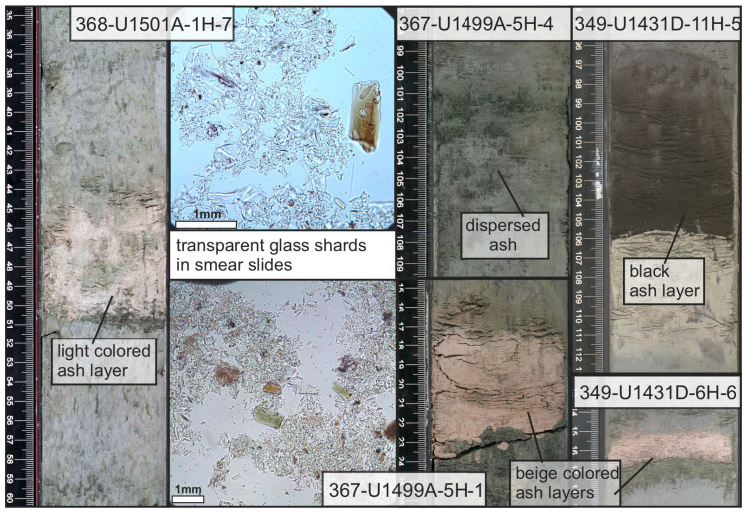

Figure F2. Core images and smear slide photographs showing different types of ash layers and dispersed ash recovered in the cores, Expeditions 349 and 367/368.

U1504, and U1505 (Figure F2). All discrete ash layers recovered during Expedition 367/368 have been investigated in this study, and the data are included in this data report.

2. Methods

2.1. Core sampling

Shipboard visual core descriptions are used to identify intervals of interest, indicating possible discrete ash layers, and samples were taken during the respective expeditions. The archive-half sections of the sediment cores were visually described on board for lithologic and sedimentary features aided by a 20× wide-field hand lens and binocular microscope. Visual inspection and smear slide analysis yielded information about variations in lithologic components, color, sedimentary structures, and occasionally drilling disturbances. Samples of discrete ash layers were then taken from the working halves during the IODP Expeditions 349 and 367/368 using mostly the standard IODP plastic 10 cm^3 scoop and tube containers.

2.2. Laboratory preparation

Marine ash samples from Expedition 349 were prepared following the methods of Blockley et al. (2005). Samples were wet sieved to remove clay, and the >25 µm fraction was retained. This was washed in 10% HCl to remove carbonates. Sodium polytungstate was used to separate the ash and mineral fractions. Each ash sample was poured into one of six predrilled holes in a 1 inch acrylic mount. Surfaces of the epoxy discs were polished and carbon coated for analysis.

Marine ash samples from Expedition 367/368 were wet sieved into different grain size fractions (63–125, 125–250, >250 µm, and, if necessary, 32–63 µm). The 63–125 µm fraction was further used for compositional analysis of glass shards by embedding 12 samples into one 1 inch predrilled acrylic mount having 12 holes with the two-component epoxy resin araldite. Afterward, the sample surfaces were polished using 9, 3, and 1 µm polish, and subsequently the tablets were carbon coated to provide discharge of the electrons during electron microprobe (EMP) measurements.

Compositional analysis of the glass shards of samples from all three expeditions was conducted by EMP and laser ablation–inductively coupled plasma–mass spectrometry (LA-ICP-MS).

2.3. Electron microprobe analyses

Glass shards (720 in total) were analyzed for major and minor elements on 55 epoxy-embedded samples (measurement of 15–40 individual shards per sample) using either a JEOL JXA 8200 wavelength dispersive EMP at the GEOMAR Helmholtz Centre for Ocean Research (Kiel, Germany) utilizing the methods of Kutterolf et al. (2011) or a JEOL JXA-8230 at the State Key Laboratory of Marine Geology at Tongji University (China).

At GEOMAR, a calibrated measuring program was used based on international standards with a 6 nA current and 10 µm diameter electron beam to minimize sodium loss. Accuracy was monitored by two measurements each on Lipari obsidian (Lipari rhyolite; Hunt and Hill, 2001) and Smithsonian basaltic standard VGA99 (Makaopuhi Lava Lake, Hawaii; Jarosewich et al., 1980) after every 60 single glass shard measurements. Standard deviations (1σ) in comparison to reference values are <2% for major and <5% for minor elements (with the exception of P_2O_5, MgO, and MnO_2 in Lipari and MnO_2 in VGA99).

At Tongji University, the analyses were performed using an accelerating voltage of 15 kV and beam current of 10 nA using a 5 µm diameter beam. Natural and synthetic mineral standards were used to calibrate all quantitative analyses, and ZAF correction was used for data reduction.

All analyses with totals >90 wt% were normalized to 100% to eliminate the effects of variable post-depositional hydration and minor deviations in focusing the electron beam. Analyses that show clear signs of microcrystal contamination (e.g., increased Al_2O_3, CaO, and Na_2O for plagioclase or increased MgO and FeO_t for olivine or pyroxene) were excluded.

2.4. Laser ablation–inductively coupled plasma–mass spectrometry

The trace element concentrations of ~130 glass shards from marine tephras (21 samples; 2–15 individual glass shard analyses per sample) were determined by LA-ICP-MS in 2018 at the Academia Sinica in Taipei, Taiwan, and at the Geochemical Analysis Unit at Macquarie University in Australia.

At the Academia Sinica, the LA-ICP-MS instrumentation comprises a 193 nm excimer laser (Teledyne CETAC Analyte G2) set to a spot size of 24–30 µm (using 5–10 J/cm^2 energy density at a 4–10 Hz repetition rate) coupled to a high-resolution ICP-MS (Agilent 7900). Following 45 s of blank acquisition, typical ablation times were around 75 s. Data reduction was performed using Version 4.0 of "real-time on-line" GLITTER software (van Achterberg et al., 2001) immediately following each ablation analysis. Individual calcium concentrations, measured by EMP, mostly on the same glass shards, were used as an internal standard to calibrate each trace element analysis. An international glass standard from the United States Geological Survey (BCR-2g; Wilson, 1997) was measured every 10 sample measurements to monitor accuracy and to correct for matrix effects and signal drift in the ICP-MS and also for differences in the ablation efficiency between sample and reference material (Günther et al., 1999). The concentrations of NIST SRM 612, needed for external calibration, were taken from Norman et al. (1996) and Jochum et al. (2011). The limit of detection (LOD) for most trace elements was generally <100 ppb. For rare earth elements, the LOD is generally around 10 ppb. The 1σ analytical precision compared to standard reference data of BCR-2g is generally better than 5% for Li, Sc, Cr, Rb, Sr, Ba, La, Ce, Pr, Nd, Sm, Eu, Dy, Er, Lu, Hf, Pb, and U and better than 10% for the rest of the trace elements (Co, Zr, Nb, Cs, Gd, Tb, Ho, Tm, Yb, Ta, and Th), except for Y (12.5%).

At Macquarie University, trace element concentrations were determined on an Agilent 7700x quadrupole ICP-MS coupled with a Photon Machines Excite 193 nm excimer laser ablation system (fitted with a two-stage HeLeX cell). Counting times were 45 s on a gas background followed by up to 45 s of ablation/analysis, depending on the size of the grain. Analyses were carried out using a spot size of 30 µm for standards and 10–40 µm for unknowns (depending on the size of the shard), a pulse rate of 5 Hz, and laser energy of ~7–9 J/cm^2. The carrier gas was He in the sample cell, with Ar added downstream. Data reduction was performed using Version 4.0 of "real-time on-line" GLITTER software (van Achterberg et al., 2001) immediately following each ablation analysis.

All of the resulting major and trace element data as well as standard analyses are provided in ANALYSES in **Supplementary material**.

3. Results

3.1. Geochemical compositions

From 55 samples that were analyzed for their major and partly for their trace element glass geochemistry, we identified 46 as tephra layers containing pyroclasts as the dominant component, whereas the others contained no measurable glass shards. Two samples were too altered/hydrated and show very low totals (<90 wt%) or very low alkali contents (Na_2O and K_2O below 2 wt%). These geochemical results cannot be used for further investigations. Several samples especially in the deeper sections of Hole U1431D are tachylitic, and microcrystals might have influenced the geochemical results (see ANALYSES in **Supplementary material**).

Overall, the tephra layers from Expedition 349 cover the geochemical range from basaltic (trachy-) andesite to trachyte and rhyolite following the total alkali versus silica diagram after LeMaitre et al. (2002) (Figure **F3A**) (2–4 wt% K_2O; 54–79 wt% SiO_2). Tephra layers from Expedition 367/368 are exclusively rhyolitic in composition (~2–3 wt% K_2O; >77 wt% SiO_2 (Figure **F3A**). All samples follow the calc-alkaline and K-rich calc-alkaline magmatic series, with one Expedition 349 sample falling into the shoshonitic series (Figure **F3B**).

3.2. Tephra ages

We applied the published age models (Li et al., 2015b; **Larsen et al.**, 2018; Jian et al., 2019) and calculated tephra ages based on the average sedimentation rates assuming a constant sedimentation rate. The sedimentation rate at Site U1431 is 50 mm/ky throughout the Pleistocene. At Site U1499, the sedimentation rate is higher, 130 mm/ky in the upper ~48 mbsf followed by a slump deposit (mass wasting event), and lower in the deeper part of the core (50–80 mm/ky) (**Larsen et al.**, 2018). However, most of the investigated tephra samples derive from above the slump. At Site U1501, the sedimentation rate during the Pleistocene is 15 mm/ky (Jian et al., 2019). The tephra ages range ~0.038–1.9 Ma at Site U1431 and ~0.028–0.8 Ma at Site U1499. Tephra layers at Sites U1501 and U1505 occur at 0.59 and ~0.87 Ma, respectively. The calculated ages of each interval are listed in ANALYSES in **Supplementary material**.

3.3. Preliminary correlations

Rhyolitic tephra layers from Hole U1501A (interval 1H-7, 48–49 cm; ~590 ka; Figure **F2**) and U1505C (interval 3H-3, 24–32 cm; ~870 ka) have indistinguishable major and trace element compositions (Figure **F3**). Visual description and comparison of the core images also strongly support correlation of these two tephra layers, but the calculated ages of the available age models do not support this correlation. We therefore assume that the sedimentation rates in the uppermost parts of Site U1505 might actually be higher (~35 mm/ky) than previously estimated.

Preliminary correlation of the marine tephra data with known eruptions and compositions from the adjacent arcs indicate different source regions along the Luzon and Bicol arcs (Figure **F3C,**

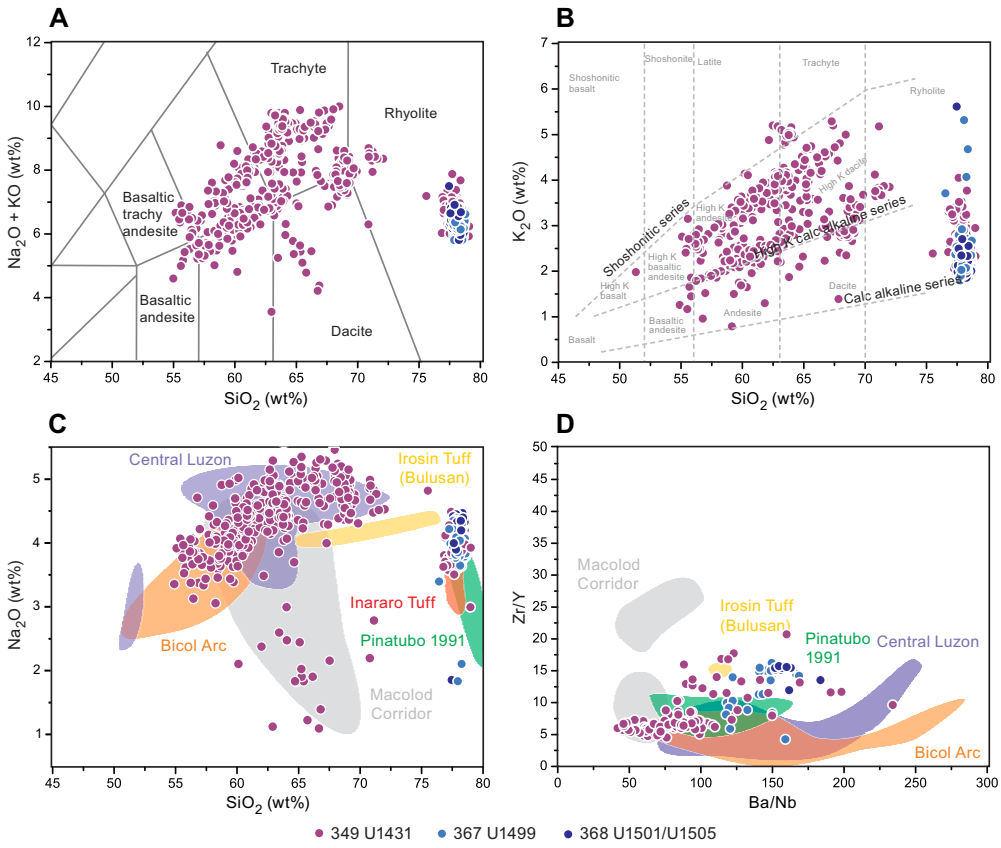

Figure F3. A. Total alkali versus silica classification diagram. B. K_2O versus SiO_2 classification diagram. C. Na_2O versus SiO_2 diagram. D. Ba/Nb versus Zr/Y ratios diagram with correlation fields. Each symbol represents a single glass shard analysis. Preliminary correlation of tephra layers to adjacent volcanic arcs and eruptions (data used to draw the correlation fields were taken from Ku et al., 2008, 2009; Mirabueno et al., 2011; McDermott et al., 2005; Vogel et al., 2006; Yumul et al., 2003; Bernard et al., 1996; Wiesner et al., 1995).

F3D). Rhyolitic marine tephra layers from Expeditions 349 and 367/368 show similarities with geochemical compositions known from Mount Pinatubo, for example the Inararo Tuff (~81 ka; Ku et al., 2008) or the 1991 eruption (Figure **F3C, F3D**). One sample from Expedition 349 shows relatively low Na_2O values (<3 wt%) that are more typical for eruptions from the Macolod Corridor (Figure **F3C**).

One tephra layer (interval 349-U1431D-1H-2, 39–41 cm; 38 ka calculated age) in the uppermost core of Site U1431 is preliminary correlated to the 41 ka Irosin Tuff from the Irosin Caldera, which is a widespread marker tephra in the SCS region (Figure **F3C, F3D**).

Another tephra layer (interval 349-U1431D-6H-1, 13–15 cm; ~827 ka) has similar major element glass composition as the layer "S" described in Core MD97-2142 (Figure **F1**), east of the drill site (Ku et al., 2009), which has an inferred age of 818 ka but a nonspecific source (Ku et al., 2009).

4. Acknowledgments

This research used samples and data provided by the International Ocean Discovery Program (IODP). IODP is sponsored by the National Science Foundation and other participating countries. We kindly acknowledge the efforts of all participating on- and offshore IODP technicians and laboratory and leading officers, Siem Offshore officers and crew, the drilling personnel, and the scientific parties of Expeditions 349 and 367/368. KD would like to thank the Australia-New Zealand IODP Consortium (ANZIC), which provided postexpedition funding for this study, and the State Key Laboratory of Marine Geology, Tongji University (No. MGK1512). ANZIC is supported by the Australian Government through the Australian Research Council's LIEF funding scheme LE140100047 and the Australian and New Zealand consortium of universities and government agencies. We appreciate thorough comments by reviewer Katharina Pank.

References

Barckhausen, U., Engels, M., Franke, D., Ladage, S., and Pubellier, M., 2014. Evolution of the South China Sea: revised ages for breakup and seafloor spreading. Marine and Petroleum Geology, 58:599–611. **https://doi.org/10.1016/j.marpetgeo.2014.02.022**

Bernard, A., Knittel, U., Weber, B., Weis, D., Albrecht, A., Hattori, K., Klein, J. and Oles, D., 1996. Petrology and geochemistry of the 1991 eruption products of Mount Pinatubo. In Newhall, C.G., and Punungbayan, R.S. (Eds.), Fire and Mud: Eruptions and Lahars of Mount Pinatubo, Philippines: Hong Kong (University of Washington Press), 767–797. **https://pubs.usgs.gov/pinatubo/bernard/**

Blockley, S.P.E., Pyne-O'Donnell, S.D.F., Lowe, J.J., Matthews, I.P., Stone, A., Pollard, A.M., Turney, C.S.M., and Molyneux, E.G., 2005. A new and less destructive laboratory procedure for the physical separation of distal glass tephra shards from sediments. Quaternary Science Reviews, 24(16):1952–1960. **https://doi.org/10.1016/j.quascirev.2004.12.008**

Briais, A., Patriat, P., and Tapponnier, P., 1993. Updated interpretation of magnetic anomalies and seafloor spreading stages in the south China Sea: implications for the Tertiary tectonics of Southeast Asia. Journal of Geophysical Research: Solid Earth, 98(B4):6299–6328. **https://doi.org/10.1029/92JB02280**

Franke, D., Savva, D., Pubellier, M., Steuer, S., Mouly, B., Auxietre, J.-L., Meresse, F., and Chamot-Rooke, N., 2014. The final rifting evolution in the South China Sea. Marine and Petroleum Geology, 58:704–720. **https://doi.org/10.1016/j.marpetgeo.2013.11.020**

Günther, D., Jackson, S.E., and Longerich, H.P., 1999. Laser ablation and arc/spark solid sample introduction into inductively coupled plasma mass spectrometers. Spectrochimica Acta Part B: Atomic Spectroscopy, 54(3–4):381–409. **https://doi.org/10.1016/S0584-8547(99)00011-7**

Hunt, J.B., and Hill, P.G., 2001. Tephrological implications of beam size–sample-size effects in electron microprobe analysis of glass shards. Journal of Quaternary Science, 16(2):105–117. **https://doi.org/10.1002/jqs.571**

Jarosewich, E., Nelen, J.A., and Norberg, J.A., 1980. Reference samples for electron microprobe analysis. Geostandards Newsletter, 4(1):43–47. **https://doi.org/10.1111/j.1751-908X.1980.tb00273.x**

Jian, Z., Larsen, H.C., Alvarez Zarikian, C.A., and the Expedition 368 Scientists, 2018. Expedition 368 Preliminary Report: South China Sea Rifted Margin. International Ocean Discovery Program. **https://doi.org/10.14379/iodp.pr.368.2018**

Jian, Z., Jin, H., Kaminski, M.A., Ferreira, F., Li, B., and Yu, P.-S., 2019. Discovery of the marine Eocene in the northern South China Sea. National Science Review, 6(5):881–885. **https://doi.org/10.1093/nsr/nwz084**

Jochum, K.P., Weis, U., Stoll, B., Kuzmin, D., Yang, Q., Raczek, I., Jacob, D.E., Stracke, A., Birbaum, K., Frick, D.A., Günther, D., and Enzweiler, J., 2011. Determination of reference values for NIST SRM 610–617 glasses following ISO guidelines. Geostandards and Geoanalytical Research, 35(4):397–429. **https://doi.org/10.1111/j.1751-908X.2011.00120.x**

Ku, Y.-P., Chen, C.-H., Newhall, C.G., Song, S.-R., Yang, T.F., Iizuka, Y., and McGeehin, J., 2008. Determining an age for the Inararo Tuff eruption of Mt. Pinatubo, based on correlation with a distal ash layer in core MD97-2142, South China Sea. Quaternary International, 178(1):138–145. **https://doi.org/10.1016/j.quaint.2007.02.025**

Ku, Y.-P., Chen, C.-H., Song, S.-R., Iizuka, Y., and Shen, J.J.-S., 2009. A 2 Ma record of explosive volcanism in southwestern Luzon: implications for the timing of subducted slab steepening. Geochemistry, Geophysics, Geosystems, 10(6):Q06017. **https://doi.org/10.1029/2009GC002486**

Kutterolf, S., Freundt, A., and Burkert, C., 2011. Eruptive history and magmatic evolution of the 1.9 kyr Plinian dacitic Chiltepe tephra from Apoyeque volcano in west-central Nicaragua. Bulletin of Volcanology, 73(7):811–831. **https://doi.org/10.1007/s00445-011-0457-0**

Larsen, H.C., Sun, Z., Stock, J.M., Jian, Z., Alvarez Zarikian, C.A., Klaus, A., Boaga, J., Bowden, S.A., Briais, A., Chen, Y., Cukur, D., Dadd, K.A., Ding, W., Dorais, M.J., Ferré, E.C., Ferreira, F., Furusawa, A., Gewecke, A.J., Hinojosa, J.L., Höfig, T.W., Hsiung, K.-H., Huang, B., Huang, E., Huang, X.-L., Jiang, S., Jin, H., Johnson, B.G., Kurzawski, R.M., Lei, C., Li, B., Li, L., Li, Y., Lin, J., Liu, C., Liu, C., Liu, Z., Luna, A., Lupi, C., McCarthy, A.J., Mohn, G., Ningthoujam, L.S., Nirrengarten, M., Osono, N., Peate, D.W., Persaud, P., Qiu, N., Robinson, C.M., Satolli, S., Sauermilch, I., Schindlbeck, J.C., Skinner, S.M., Straub, S.M., Su, X., Tian, L., van der Zwan, F.M., Wan, S., Wu, H., Xiang, R., Yadav, R., Yi, L., Zhang, C., Zhang, J., Zhang, Y., Zhao, N., Zhong, G., and Zhong, L., 2018. Expedition 367/368 summary. In Sun, Z., Jian, Z., Stock, J.M., Larsen, H.C., Klaus, A., Alvarez Zarikian, C.A., and the Expedition 367/368 Scientists, South China Sea Rifted Margin. Proceedings of the International Ocean Discovery Program, 367/368: College Station, TX (International Ocean Discovery Program). **https://doi.org/10.14379/iodp.proc.367368.101.2018**

Le Maitre, R.W., Streckeisen, A., Zanettin, B., Le Bas, M.J., Bonin, B., and Bateman, P., 2002. Igneous Rocks: A Classification and Glossary of Terms: Recommendations of the International Union of Geological Sciences Subcommission on the Systematics of Igneous Rocks: Cambridge (Cambridge University Press). **https://doi.org/10.1017/CBO9780511535581**

Li, C., and Song, T., 2012. Magnetic recording of the Cenozoic oceanic crustal accretion and evolution of the South China Sea basin. Chinese Science Bulletin, 57(24):3165–3181. **https://doi.org/10.1007/s11434-012-5063-9**

Li, C.-F., Li, J., Ding, W., Franke, D., Yao, Y., Shi, H., Pang, X., Cao, Y., Lin, J., Kulhanek, D.K., Williams, T., Bao, R., Briais, A., Brown, E.A., Chen, Y., Clift, P.D., Colwell, F.S., Dadd, K.A., Hernández-Almeida, I., Huang, X.-L., Hyun, S., Jiang, T., Koppers, A.A.P., Li, Q., Liu, C., Liu, Q., Liu, Z., Nagai, R.H., Peleo-Alampay, A., Su, X., Sun, Z., Tejada, M.L.G., Trinh, H.S., Yeh, Y.-C., Zhang, C., Zhang, F., Zhang, G.-L., and Zhao, X., 2015a. Seismic stratigraphy of the central South China Sea basin and implications for neotectonics. Journal of Geophysical Research: Solid Earth, 120(3):1377–1399. **https://doi.org/10.1002/2014JB011686**

Li, C.-F., Lin, J., Kulhanek, D.K., Williams, T., Bao, R., Briais, A., Brown, E.A., Chen, Y., Clift, P.D., Colwell, F.S., Dadd, K.A., Ding, W., Almeida, I.H., Huang, X.-L., Hyun, S., Jiang, T., Koppers, A.A.P., Li, Q., Liu, C., Liu, Q., Liu, Z., Nagai, R.H., Peleo-Alampay, A., Su, X., Sun, Z., Tejada, M.L.G., Trinh, H.S., Yeh, Y.-C., Zhang, C., Zhang, F., Zhang, G.-L., and Zhao, X., 2015b. Expedition 349 summary. In Li, C.-F., Lin, J., Kulhanek, D.K., and the Expedition 349 Scientists, South China Sea Tectonics. Proceedings of the International Ocean Discovery Program, 349: College Station, TX (International Ocean Discovery Program). **https://doi.org/10.14379/iodp.proc.349.101.2015**

Li, C.-F., Pinxian, W., Franke, D., Lin, J., and Jun, T., 2012. Unlocking the opening processes of the South China Sea. Scientific Drilling, 14:55–59. **https://doi.org/10.2204/iodp.sd.14.07.2012**

Li, P., Yu, X., Li, H., Qiu, J., and Zhou, X., 2013. Jurassic–Cretaceous tectonic evolution of Southeast China: geochronological and geochemical constraints of Yanshanian granitoids. International Geology Review, 55(10):1202–1219. **https://doi.org/10.1080/00206814.2013.771952**

McDermott, F., Jr., F.G.D., Defant, M.J., Turner, S., and Maury, R., 2005. The petrogenesis of volcanics from Mt. Bulusan and Mt. Mayon in the Bicol arc, the Philippines. Contributions to Mineralogy and Petrology, 150(6):652–670. **https://doi.org/10.1007/s00410-005-0042-7**

Mirabueno, M.H.T., Okuno, M., Torii, M., Danhara, T., Laguerta, E.P., Newhall, C.G., and Kobayashi, T., 2011. The Irosin co-ignimbrite ash-fall deposit: a widespread tephra marker in the Bicol arc, south Luzon, Philippines. Quaternary International, 246(1–2):389–395. **https://doi.org/10.1016/j.quaint.2011.08.043**

Norman, M.D., Pearson, N.J., Sharma, A., and Griffin, W.L., 1996. Quantitative analysis of trace elements in geological materials by laser ablation ICPMS: instrumental operating conditions and calibration values of NIST glasses. Geostandards Newsletter, 20(2):247–261. **https://doi.org/10.1111/j.1751-908X.1996.tb00186.x**

Pubellier, M., Fredy, G., Loevenbruck, A., and Chorowicz, J., 2000. Recent deformation at the junction between the North Luzon block and the Central Philippines from ERS-1 Images. Island Arc, 9:598–610. **https://doi.org/10.1111/j.1440-1738.2000.00305.x**

Ryan, W.B.F., Carbotte, S.M., Coplan, J.O., O'Hara, S., Melkonian, A., Arko, R., Weissel, R.A., Ferrini, V., Goodwillie, A., Nitsche, F., Bonczkowski, J., and Zemsky, R., 2009. Global multi-resolution topography synthesis. Geochemistry, Geophysics, Geosystems, 10(3):Q03014. **https://doi.org/10.1029/2008GC002332**

Sun, W., 2016. Initiation and evolution of the South China Sea: an overview. Acta Geochimica, 35(3):215–225. **https://doi.org/10.1007/s11631-016-0110-x**

Sun, Z., Stock, J., Jian, Z., McIntosh, K., Alvarez-Zarikian, C.A., and Klaus, A., 2016. Expedition 367/368 Scientific Prospectus: South China Sea Rifted Margin. International Ocean Discovery Program. **https://doi.org/10.14379/iodp.sp.367368.2016**

van Achterberg, E., Ryan, C. and Griffin, W., 2001. GLITTER Version 4 User's Manual On-Line Interactive Data Reduction for the LA-ICPMS Microprobe: North Ryde, Australia (Macquarie Research Ltd.).

Vogel, T.A., Flood, T.P., Patino, L.C., Wilmot, M.S., Maximo, R.P.R., Arpa, C.B., Arcilla, C.A., and Stimac, J.A., 2006. Geochemistry of silicic magmas in the Macolod Corridor, SW Luzon, Philippines: evidence of distinct, mantle-

derived, crustal sources for silicic magmas. Contributions to Mineralogy and Petrology, 151(3):267–281. **https://doi.org/10.1007/s00410-005-0050-7**

Wiesner, M.G., Wang, Y., and Zheng, L., 1995. Fallout of volcanic ash to the deep South China Sea induced by the 1991 eruption of Mount Pinatubo (Philippines). Geology, 23(10):885–888. **https://doi.org/10.1130/0091-7613(1995)023<0885:FOVATT>2.3.CO;2**

Wilson, S.A., 1997. The collection, preparation and testing of USGS reference material BCR-2, Columbia River, basalt. US Geological Survey Open-File Report, 98-00x.

Xu, Y., Wei, J., Qiu, H., Zhang, H., and Huang, X., 2012. Opening and evolution of the South China Sea constrained by studies on volcanic rocks: preliminary results and a research design. Chinese Science Bulletin, 57(24):3150–3164. **https://doi.org/10.1007/s11434-011-4921-1**

Yumul, G.P., Jr., Dimalanta, C.B., Tamayo, R.A., Jr., and Maury, R.C., 2003. Collision, subduction and accretion events in the Philippines: a synthesis. Island Arc, 12(2):77–91. **https://doi.org/10.1046/j.1440-1738.2003.00382.x**

Zhou, D., Sun, Z., Chen, H.Z., Xu, H.H., Wang, W.Y., Pang, X., Cai, D.S., and Hu, D.K., 2008. Mesozoic paleogeography and tectonic evolution of South China Sea and adjacent areas in the context of Tethyan and Paleo-Pacific interconnections. Island Arc, 17(2):186–207. **https://doi.org/10.1111/j.1440-1738.2008.00611.x**

Zhou, T., and Li, H., 2000. Force balance modelling for agglomerating fluidization of cohesive particles. Powder Technology, 111(1–2):60–65. **https://doi.org/10.1016/S0032-5910(00)00241-2**